

The Sensitivity Limit of Rydberg Electrometry via Fisher-Information-Optimized Slope Detection

Chenrong Liu

*College of Metrology Measurement and Instrument,
China Jiliang University, Hangzhou, 310018 China and*

Research Center for Novel Computing Sensing and Intelligent Processing, Zhejiang Lab, Hangzhou, 310000 China

Mingti Zhou, Chuang Li, and Ying Dong*
*College of Metrology Measurement and Instrument,
China Jiliang University, Hangzhou, 310018 China*

Xiang Lv

Research Center for Novel Computing Sensing and Intelligent Processing, Zhejiang Lab, Hangzhou, 310000 China

Bihu Lv†

*Research Center for Novel Computing Sensing and Intelligent Processing, Zhejiang Lab, Hangzhou, 310000 China and
Department of Scientific Facilities Development and Management Zhejiang Lab, Hangzhou, 310000 China*

(Dated: March 18, 2025)

We present a comprehensive theoretical study of the Fisher information and sensitivity of a Rydberg-atom-based microwave-field electrometer within the framework of slope detection. Instead of focusing on the Autler-Townes (AT) splitting of the electromagnetically induced transparency (EIT) spectrum of the probe laser, we shift the analytical focus to the transmitted power response to the signal microwave to be measured. Through meticulous analysis of the signal-to-noise ratio (SNR) in transmitted light power, we naturally derive the desired sensitivity. Crucially, we demonstrate that laser-intrinsic noise, rather than the relaxation of the atomic system, predominantly governs the uncertainty in microwave measurement. Based on this, the Fisher information, which characterizes the precision limit of microwave measurement, is deduced. Considering only non-technical relaxation processes and excluding controllable technical relaxations, the optimal sensing conditions are numerically analyzed from the perspective of maximizing the Fisher information. The results reveal that the sensitivity of the electrometer under such conditions can reach $\text{sub-nV}/(\text{cm}\sqrt{\text{Hz}})$. Our work provides a rigorous quantitative characterization of the performance of the Rydberg-atom-based microwave-field electrometer and presents an effective strategy for optimizing its performance.

I. INTRODUCTION

In recent years, the utilization of Rydberg atoms for sensing microwave (MW) electric fields has garnered substantial attention due to their exceptional sensitivity to external electric fields [1, 2]. The strength of the microwave electric field can be precisely determined by measuring the frequency separation of the Autler-Townes (AT) splitting within the electromagnetically induced transparency (EIT) spectrum [3]. Over the past decade, significant progress has been made in Rydberg-atom-based microwave electrometers that leverage the EIT-AT effect [3–9]. However, the slope detection method [10], which is commonly used in quantum sensing, has not received the deserved recognition in this realm, in contrast to the EIT-AT effect sensing strategy.

Slope detection in sensors focuses on the derivative of the directly measured variable with respect to the quantity of interest at a well-selected reference point [10]. In

this context, the response of the directly measured variable scales linearly with any infinitesimal variation in the quantity of interest. When applied to Rydberg-atom-based microwave field electrometers, this approach enables the detection of microwave fields that are orders of magnitude weaker than the reference local field [11]. However, a quantitative performance description for this type of electrometer in slope detection remains elusive. Notably, Fisher information defines the theoretical upper limit of measurement precision in parameter estimation frameworks [12, 13], providing a quantitative assessment of noise that facilitates the evaluation of the sensor’s potential performance and avenues for improvement [10].

On one hand, conventional EIT-AT detection quantifies microwave fields via the Autler-Townes splitting interval $\Delta_{\text{AT}} \propto \Omega_s$ in the probe transmission spectrum [2, 3]. The measurement errors thus predominantly arise from the reconstruction of the EIT spectrum [3], rather than probe laser noise. The EIT spectrum profile of the transmitted probe laser is influenced by various relaxation processes within the system, including decay relaxation processes such as spontaneous emission [14] and thermal radiation from the external environment [15];

* yingdong@cjl.u.edu.cn

† lvbh@zhejianglab.com

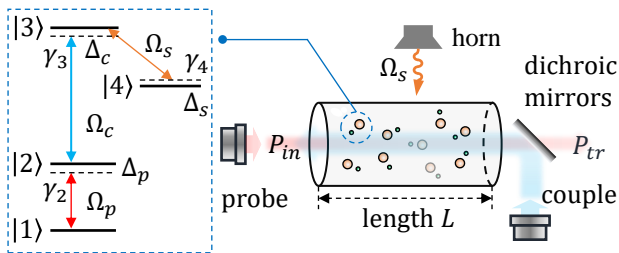


FIG. 1. (Color online) Schematic diagram of the Rydberg-atom-based microwave-field electric sensing.

The probe light enters the atom vapor cell from the left side and exits from the right side. The cell has a length of L . The initial power of the probe laser is P_{in} , and the transmitted power P_{tr} is used to reconstruct the EIT spectrum as a function of detuning Δ_c . A horn feed microwave with Rabi frequency Ω_s is introduced into the cell, resulting in EIT-AT splitting. The energy level setup can be seen in Table I.

and dephasing relaxation processes such as atom-atom collisions [16], transit time [17, 18], laser spectrum energy density with a certain linewidth [19–21], Doppler effect [21, 22], and laser power broadening [14]. These processes broaden the EIT spectral width [6, 14], thus significantly reducing the minimal resolution of the EIT-AT splitting and rendering the sensitivity of EIT-AT effect-based detection highly susceptible to these relaxation mechanisms [6]. On the other hand, slope detection focuses on the response of the transmitted probe laser to the microwave field at a well-selected reference point. Here, the EIT spectrum is not critical; instead, the probe laser’s response and its derivative with respect to the microwave field are the primary factors. This allows the measurement precision of the Rydberg-atom-based electrometer to approach the shot noise limit in principle, thereby achieving superior measurement performance.

The signal-to-noise ratio (SNR) is a critical metric in both classical and quantum sensing, directly influencing measurement sensitivity and reliability. Defined as the ratio of signal power to noise power, the SNR serves as a measure of the quality of the microwave signal to be measured. In this study, we focus on slope detection and determine its measurement sensitivity for microwaves, bridging the relationship between SNR and Fisher information. Errors in microwave measurement propagate from errors in the transmitted probe laser power, while the aforementioned relaxation processes affect the attenuation of the transmitted probe laser power, as illustrated in Fig. (1). In this work, Fisher information in slope detection is estimated as the precision limit for measuring the microwave electric field strength. The SNR is defined in terms of the transmitted probe laser power, enabling straightforward calculation of sensitivity. The sensitivity limit thus can be obtained through the optimization of Fisher information, which covers the experimental results. While building upon M. Jing’s pioneering hetero-

dyne scheme [11], our Fisher-information approach reveals previously unexplored optimization pathways. Finally, a numerical presentation of the Fisher information and sensitivity of the Rydberg-atom-based microwave-field electrometer with slope detection is carried out. The special case corresponding to zero temperature ($T \rightarrow 0$) is also analytically investigated.

TABLE I. The collection of parameters setup in numerical computation for ^{133}Cs atoms (also see in Refs. 11 and Appendix C).

Laser		Atom		Light-Atom	
Ω_0	6.947 GHz	\mathcal{N}_0^a	$4.894 \times 10^{16} \text{ m}^{-3}$	L^b	0.05 m
λ_p	852 nm	μ_{21}	$2.5817 ea_0^c$	$\Omega_0/2\pi$	to be solved
λ_c	510 nm	μ_{32}	$0.0186 ea_0$	$\Omega_p/2\pi$	7.9254 MHz
P_{c0}	34 mW	μ_s	$1443.4498 ea_0$	$\Omega_c/2\pi$	0.4806 MHz
w_{c0}	1 mm	$\gamma_2/2\pi$	5.223 MHz	$\Delta_L/2\pi$	0 MHz
P_{p0}^d	120 μW	$\gamma_3/2\pi$	3.982 kHz	$\Delta_p/2\pi$	0 MHz
w_{p0}^e	0.85 mm	$\gamma_4/2\pi$	1.745 kHz	$\Delta_c/2\pi$	[-50, 50] MHz

^a The temperature is setup in $T = 298.15\text{K}$ (i.e., 25°), and atom number density can be calculated [23]

^b The length of the atom vapor cell

^c The transition dipole matrix element of ^{133}Cs atom: μ_{21} for transition $6S_{1/2}(F=4) \rightarrow 6P_{3/2}(F'=5)$, μ_{32} for transition $6P_{3/2}(F=5) \rightarrow 4D_{5/2}$, μ_{43} for transition $4D_{5/2} \rightarrow 4F_{3/2}$, in unit of $ea_0 = 8.47835362554076610^{-30} \text{ C} \cdot \text{m}$. (See in Ref. 23)

^d Initial power of probe laser, similar for couple laser.

^e The waist radius of probe laser, similar for couple laser.

II. FISHER INFORMATION AND SENSITIVITY IN SLOPE DETECTION

In the following, we firstly present the basic framework of slope detection in Rydberg-atom-based microwave-field electric sensing. Secondly, theoretically discussion and determination of the Fisher information by error propagation and the sensitivity through SNR of the directly measured probe laser power will be carried out. We establishes the connection between them, which reveals the strategy to reach the optimal detection condition of the Rydberg-atom-based microwave-field electrometer by finding the maximum of Fisher information.

A. Slope Detection

The core apparatus of the electrometer considered here is the atom vapor cell, as depicted in Fig. 1, with an insert showing the atomic level diagram. We choose ^{133}Cs as the working atom (Ref. 11). The probe and coupling laser beams counter-propagate through the ^{133}Cs atom vapor cell at room temperature. The incident power of the probe laser is denoted as P_{in} , and the transmitted power is P_{tr} , which are related by

$$P_{tr} = P_{in} \cdot \eta(\Omega_s), \quad (1)$$

where $\eta(\Omega_s)$ is the transmission of the probe laser, characterizing the attenuation of the probe laser through the cell [11, 20, 24], and Ω_s is the microwave Rabi frequency. The average photon number of the probe laser, prepared in an optical coherence state $|\alpha\rangle$, satisfies

$$\bar{n}_{tr} = \bar{n}_{in} \cdot \eta(\Omega_s), \quad (2)$$

where Ω_s is the microwave Rabi frequency. Through the secondary quantization of the propagating electromagnetic field in the coherence state $|\alpha\rangle$, the incident average photon number is $\bar{n}_{in} = \bar{n}_0 = \langle \alpha | \hat{a}^\dagger \hat{a} | \alpha \rangle$, while the transmitted average photon number is \bar{n}_{tr} , and its state becomes $|\alpha\sqrt{\eta}\rangle$ (see details in Appendix A).

Slope detection in Rydberg-atom-based microwave-field electric sensing is similar to Ramsey measurements in magnetometry (see details in Ref. [10]). For an arbitrarily small deviation of the microwave Rabi frequency $\delta\Omega_s$ around a reference Rabi frequency Ω_0 [10], it induces a corresponding change in the transmitted power as described by Eq. (1):

$$\delta P_{tr} = \left. \frac{\partial P_{tr}}{\partial \Omega_s} \right|_{\Omega_s=\Omega_0} \delta\Omega_s = P_{tr} \frac{\partial \ln \eta}{\partial \Omega_0} \delta\Omega_s, \quad (3)$$

and the derivative of transmitted power over microwave is denoted as

$$k_p = P_{tr} \frac{\partial \ln \eta}{\partial \Omega_0}, \quad (4)$$

where the signal microwave is $\Omega_s = \delta\Omega_s + \Omega_0$, and $\delta\Omega_s \ll \Omega_0$ acts as a perturbation of Ω_0 . Notably, the reference microwave Ω_0 can be carefully chosen to optimize the response performance of the Rydberg-atom-based microwave-field electrometer, as discussed below. Therefore, the perturbation signal $\delta\Omega_s$ around the reference microwave Ω_0 can be determined with a certain measurement sensitivity through the directly measured probe laser power. The amplitude of this perturbation microwave electric field is given by

$$\delta E_s = \frac{\hbar}{\mu_s} \delta\Omega_s, \quad (5)$$

where μ_s is the transition dipole moment between Rydberg states [2]. Thus, Rydberg-atom-based superheterodyne detection [11] is a special case of slope detection, although the perturbation microwave $\delta\Omega_s$ need not be another microwave distinct from the reference Ω_0 .

B. Fisher Information

The measurement error of the transmitted probe laser power P_{tr} originates from the laser noise, including amplitude and phase noise [25], while the atomic relaxations inherent in the system only affect the attenuation η for dilute ^{133}Cs atom vapor, which is always true in room temperature [23]. The amplitude noise can be reduced

using high-performance active power stabilization techniques [26] to the shot noise level or even below [25, 27], while the phase noise will not contribute in laser power measurement. We thus consider only the shot noise limit of probe laser measurement in the follows. The power spectral density (PSD) [25] of the transmitted probe laser in the shot noise limit can be expressed as

$$\text{PSD} = \sqrt{2\hbar\omega_p P_{tr}}, \quad (6)$$

where ω_p is the optical frequency and λ_p is its wavelength. This gives the power fluctuation of the probe laser

$$\sigma_{P_{tr}} = \text{PSD} \cdot \sqrt{B} = \sqrt{\frac{\hbar\omega_p P_{tr}}{\tau}}, \quad (7)$$

where $B = 1/2\tau$ is the spectrum bandwidth, τ is sample times. See Appendix A for details. This fluctuation results in the power measurement error and propagates to the microwave to be measured through Eq. (3) as

$$\sigma_{\Omega_s} = \frac{\sigma_{P_{tr}}}{\left| \frac{\partial P_{tr}}{\partial \Omega_s} \right|_{\Omega_s=\Omega_0}} = \left(\sqrt{\bar{n}_{tr}} \left| \frac{\partial \ln \eta}{\partial \Omega_0} \right| \right)^{-1}. \quad (8)$$

The Cramér-Rao inequality [10, 28] claims that the measurement error of the microwave to be measured will not be infinitesimal but has a lower bound

$$\Delta\Omega_s = \sqrt{\text{Var}[\Omega_s]} \geq \frac{\left| \frac{\partial P_{tr}}{\partial \Omega_0} \right|}{\sqrt{F(\Omega_s)}}, \quad (9)$$

where $F(\Omega_s)$ is the Fisher information. Atomic relaxations and probe laser shot noise determine the measurement accuracy from the dynamics framework, so the error bound $\Delta\Omega_s = \sigma_{\delta\Omega_s}$ gives the Fisher information from Eqs. (8) and (B1) as

$$F(\Omega_s) = \bar{n}_{tr} \left(\frac{\partial \ln \eta}{\partial \Omega_0} \right)^2, \quad (10)$$

which is of dependence on the reference microwave Ω_0 rather on perturbation $\delta\Omega_s$. This characterizes the lower bound of measurement precision limited by the system noise. Beside, this Fisher information is equivalent to that from parameter estimation theory, see details in Appendix B.

C. The Sensitivity

The signal-to-noise ratio (SNR) is a commonly employed metric for determining the sensitivity of a sensor. Naturally, the Rydberg-atom-based electrometer is no exception. By leveraging the directly measured probe laser power, we can quantify its SNR [10] by dividing the power signal as expressed in Eq. (3) by its fluctuation as given in Eq. (7), yielding:

$$\text{SNR} = \frac{\delta P_{tr}}{\sigma_{P_{tr}}} = \sqrt{\bar{n}_{tr}} \left| \frac{\partial \ln \eta}{\partial \Omega_0} \right| \delta\Omega_s. \quad (11)$$

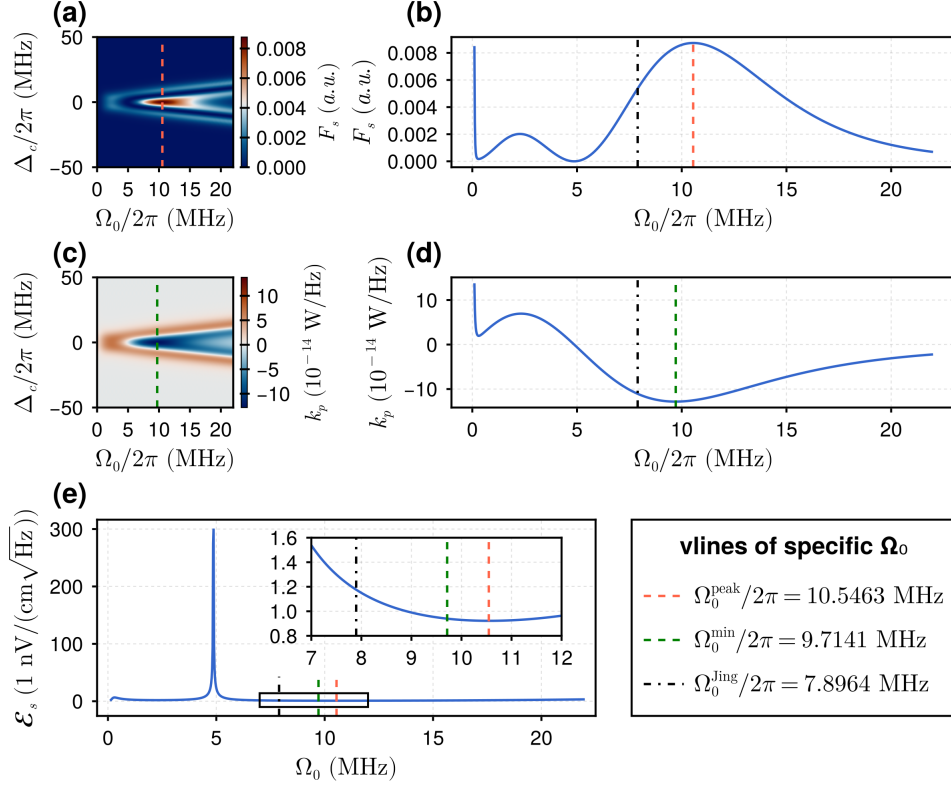


FIG. 2. (Color online) **Fisher information and sensitivity characteristics.** (a) Fisher information F_s [Eq. (10)] as functions of reference microwave Rabi frequency Ω_0 and coupling detuning Δ_c , in $\Delta_p = \Delta_s = 0$. (c) Corresponding transmitted power derivative k_p [Eq. (4)]. (b,d) Cross-sectional profiles at $\Delta_c = 0$ with vertical lines marking: dashed orange - F_s maximum $\Omega_0^{\text{peak}}/2\pi = 10.5463$ MHz, dashed green - k_p minimum $\Omega_0^{\text{min}}/2\pi = 9.7141$ MHz, dash-dotted black - local microwave Rabi frequency $\Omega_0^{\text{jing}}/2\pi = 7.8964$ MHz in Ref. [11]. (e) Sensitivity \mathcal{E}_s versus Ω_0 at $\Delta_c = 0$, in which singularity can occur at about $\Omega_0/2\pi \approx 5$ MHz as the zeros of Fisher information F_s . A legend of vertical lines in the subplot (e) and its insert which is the as that in (b,d) is presented at rightside of (e). Parameters from Table I replicate experimental conditions in Ref. [11].

The minimal detectable microwave, noting $\delta\Omega_s = \Omega_s - \Omega_0$ and taking into account Eq. (10), is thus naturally given in SNR= 1 condition by:

$$[\delta\Omega_s]_{\min} = [\delta\Omega_s]_{\text{SNR}=1} = \frac{1}{\sqrt{F(\Omega_s)}}. \quad (12)$$

Furthermore, to ensure the sensitivity of the microwave Ω_s measurement is time-independent, we set the sample time $\tau = 1$ [10], which is indeed the definition of sensitivity, resulting in:

$$\mathcal{E}_s = \frac{\hbar}{\mu_s} [\delta\Omega_s]_{\min} \cdot \sqrt{\tau} = \frac{\hbar}{\mu_s} \frac{1}{\sqrt{\frac{P_{\text{tr}}}{\hbar\omega_p} \left| \frac{\partial \ln \eta}{\partial \Omega_0} \right|}}, \quad (13)$$

which is expressed in the desired unit of $\text{V}/(\text{m}\sqrt{\text{Hz}})$. It is evident that

$$\mathcal{E}_s \propto \frac{1}{\sqrt{F(\Omega_s)}},$$

suggesting that the optimal sensitivity can be attained when the Fisher information is maximized. Through

this, we rigorously and seamlessly establish a connection between the sensitivity and the Fisher information for Rydberg-atom-based microwave-field electrometer, along with their theoretical descriptions in an elegant manner. This affords us a means to optimize the performance of the Rydberg-atom-based microwave-field electrometer.

III. NUMERICAL PRESENTATION

The Fisher information [Eq. (10)] and the sensitivity [Eq. (13)] are both general, since we have not yet delved into any specific details regarding the system, aside from the laser shot noise. Without loss of generality, we will focus our discussion in the following solely on the non-technical relaxations in the attenuation η , which encompass spontaneous emission, thermal radiation from the warm external environment, atom-atom collision, laser power broadening, and the Doppler effect. The transit time dephasing can be mitigated by increasing the waist radius w_0 of the laser [11, 18]. The laser spectrum linewidth can also be reduced to the order of mHz or even

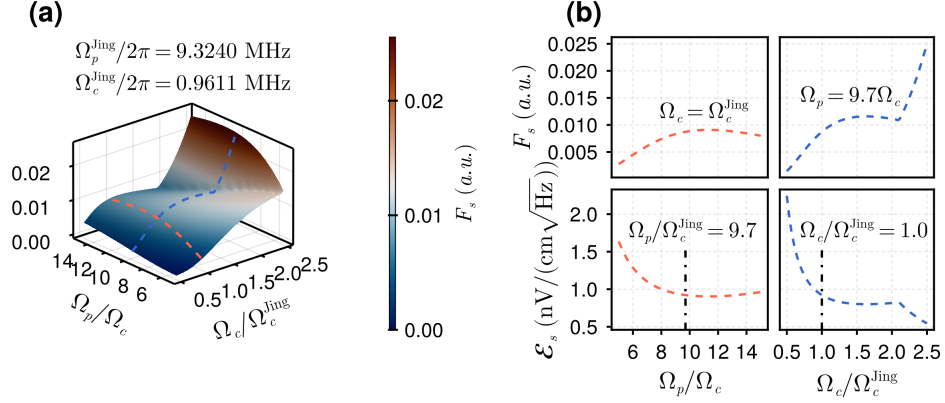


FIG. 3. **(Color online) Sensitivity optimization via Fisher information.** (a) 3D surface plot of the maximum F_s over reference microwave Ω_0 just like in Fig. 2(b) when fixing the normalized coupling $\Omega_c/\Omega_c^{\text{Jing}}$ and the ratios Ω_p/Ω_c at $\Delta_c = 0$. Red/blue curves represent orthogonal cross-sections using Table I parameters from Ref. [11]. (b) Corresponding cross-sectional profiles of Fisher information F_s and sensitivity \mathcal{E}_s showing optimal sensing condition that is of Ω_p and Ω_c dependence, which can be obtained further by parameter tuning.

Hz [11, 29–32]. Consequently, the dephasing induced by a narrow linewidth laser with mHz or even Hz can be disregarded. Details about all involved relaxation and their Lindblad operator can be seen in Appendix. C.

A. Decay and Dephasing

First of all, the attenuation η is what we want to obtain and is of critics for Fisher information and sensitivity discussion, it can be solved through master equation. Notably, the atom vapor can be treated as linear medium for probe and couple laser. The susceptibility χ arising from the polarization of atom vapor by the electric field of the probe laser can be derived as [14, 20]

$$\chi = -\frac{2\mathcal{N}_0\mu_{21}^2}{\epsilon_0\hbar\Omega_p}\rho_{21} = -C\rho_{21}, \quad (14)$$

where \hbar is the reduced Planck constant, μ_{21} is the dipole matrix element of the transition $|1\rangle \rightarrow |2\rangle$ as illustrated in Fig. 1, and \mathcal{N}_0 is the ^{133}Cs atom density in the cell determined by the saturation vapor pressure equation [23], Ω_p is the Rabi frequencies of the probe light. The probe laser attenuation η [33] characterizes the laser power decay can be expressed as

$$\eta(\Omega_s) = \exp\left\{-\frac{2\pi L}{\lambda_p}\text{Im}[\chi(\Omega_s)]\right\}, \quad (15)$$

The density matrix element ρ_{21} can be solved from the master equation [14]

$$\frac{\partial\tilde{\rho}}{\partial t} = \frac{1}{i\hbar}[\tilde{H}, \tilde{\rho}] + \mathcal{L}_{\text{decay}}\tilde{\rho} + \mathcal{L}_{\text{deph}}\tilde{\rho}, \quad (16)$$

in steady-state condition $\partial\tilde{\rho}/\partial t = 0$ and $\text{tr}[\tilde{\rho}] = 1$, where $\mathcal{L}_{\text{decay}}$ and $\mathcal{L}_{\text{deph}}$ are the Lindblad operator of the decay and dephasing relaxation respectively. The Hamiltonian by Rotating Wave Approximation (RWA) and frame rotation [14] is

$$\tilde{H} = \frac{\hbar}{2} \begin{bmatrix} 0 & \Omega_p & 0 & 0 \\ \Omega_p & -2\Delta_p & \Omega_c & 0 \\ 0 & \Omega_c & -2(\Delta_p + \Delta_c) & \Omega_s \\ 0 & 0 & \Omega_s & -2(\Delta_p + \Delta_c - \Delta_s) \end{bmatrix}, \quad (17)$$

where Ω_p , Ω_c , and Ω_s are the Rabi frequencies of the probe light, couple light, and microwave, respectively, and

$$\begin{aligned} \Delta_p &= \omega_1 + \omega_p - \omega_2, \\ \Delta_c &= \omega_2 + \omega_c - \omega_3, \\ \Delta_s &= \omega_4 + \omega_s - \omega_3 \end{aligned}$$

are the corresponding detuning. The level diagram can be seen in Fig. 1. The spontaneous emission, thermal radiation from the warm external environment contribute to the decay relaxation, which cause change in the energy level population. The atom-atom collision, laser power broadening, and the Doppler effect lead to dephasing, where the atomic energy level population remains unchanged but the Bloch precession pace is out of sync (de-synchronize) [14]. The decay dissipation term for the selected warm Cs atomic vapor by Lindblad operator can be derived as

$$\mathcal{L}_{decay}\tilde{\rho} = \begin{bmatrix} \gamma_2\rho_{22} + \gamma_4\rho_{44} & -\frac{\gamma_2}{2}\rho_{12} & -\frac{\gamma_3}{2}\rho_{13} & -\frac{\gamma_4}{2}\rho_{14} \\ -\frac{\gamma_2}{2}\rho_{21} & \gamma_3\rho_{33} - \gamma_2\rho_{22} & -\frac{\gamma_2+\gamma_3}{2}\rho_{23} & -\frac{\gamma_2+\gamma_4}{2}\rho_{24} \\ -\frac{\gamma_3}{2}\rho_{31} & -\frac{\gamma_3+\gamma_2}{2}\rho_{32} & -\gamma_3\rho_{33} & -\frac{\gamma_3+\gamma_4}{2}\rho_{34} \\ -\frac{\gamma_4}{2}\rho_{41} & -\frac{\gamma_4+\gamma_2}{2}\rho_{42} & -\frac{\gamma_4+\gamma_3}{2}\rho_{43} & -\gamma_4\rho_{44} \end{bmatrix}, \quad (18)$$

where $\gamma_2, \gamma_3, \gamma_4$ are the effective decay rate of $|2\rangle, |3\rangle, |4\rangle$ respectively [15]. The dephasing dissipation term induced by atom-atom collision can similarly [34] be obtained as

$$\mathcal{L}_{deph}\tilde{\rho} = \begin{bmatrix} 0 & 0 & -\Gamma_{c3}\rho_{13} & -\Gamma_{c4}\rho_{14} \\ 0 & 0 & 0 & 0 \\ -\Gamma_{c3}\rho_{31} & 0 & 0 & 0 \\ -\Gamma_{c4}\rho_{41} & 0 & 0 & 0 \end{bmatrix}, \quad (19)$$

where Γ_{c3}, Γ_{c4} are the collision dephasing rate of $|3\rangle, |4\rangle$ to $|1\rangle$. The probe laser power broaden the atom transition rate, but can be embedded into the master equation through Ω_p , leading to the transit rate γ_2 of the transition $|2\rangle \rightarrow |1\rangle$ modification as

$$\gamma'_2 = \gamma_2 \sqrt{1 + \frac{2\Omega_p^2}{\gamma_2^2}}, \quad (20)$$

where the modified term relate to the saturation intention (see details in Ref. [14]), which can be omitted for weak probe laser. The Doppler effect shall be incorporated by Boltzmann average [21] of density matrix element ρ_{21} , see details in Appendix. C. Therefore, the dephasing related dissipation term consensus only the atom-atom collision in $\mathcal{L}_{deph}\tilde{\rho}$ for non-technical relaxation as claimed prevail.

On the other hand, in the limit as $T \rightarrow 0^\circ\text{C}$, the atom-atom collision and the Doppler effect vanish. Additionally, considering that $\gamma_3, \gamma_4 \ll \gamma_2$, the density matrix element ρ_{21} can be analytically solved from the master equation [Eq. (16)] under steady-state conditions. It can be expressed under $\Delta_p = \Delta_L = 0$ as

$$\rho_{21} = \frac{B(\Omega_s^2 - 4\Delta_c^2)\Omega_c\Delta_c}{\Omega_s^4 + 2(\Gamma_0^2 - 4\Delta_c^2)\Omega_s^2 + 4(\Gamma_1^2 + 4\Delta_c^2)\Delta_c^2} - i \frac{A(\Omega_s^2 - 4\Delta_c^2)^2}{\Omega_s^4 + 2(\Gamma_0^2 - 4\Delta_c^2)\Omega_s^2 + 4(\Gamma_1^2 + 4\Delta_c^2)\Delta_c^2} \quad (21)$$

where $A = \frac{\gamma_2\Omega_p}{\gamma_2^2 + 2\Omega_p^2}$, $B = \frac{2\Omega_c\Omega_p}{\gamma_2^2 + 2\Omega_p^2}$ are dimensionless, and

$$\Gamma_0 = \Omega_p \sqrt{\frac{2(\Omega_c^2 + \Omega_p^2)}{\gamma_2^2 + 2\Omega_p^2}},$$

$$\Gamma_1 = \sqrt{\frac{(\Omega_c^2 + \Omega_p^2)^2 + \Omega_p^4}{\gamma_2^2 + 2\Omega_p^2}}$$

are of frequency units [11], the Γ_1 is EIT full width at half maxima when $\Omega_s = 0$ that can be checked easily. The modification of $\gamma_2 \rightarrow \gamma'_2$ is obvious in above expression.

Thus, in this context, the attenuation

$$\eta(\Omega_s) = \exp \left\{ -\frac{2\pi L}{\lambda_p} C' \Lambda(\Omega_p, \Omega_c, \Omega_s, \Delta_c) \right\}, \quad (22)$$

where $C' = \frac{2N_0\mu_{21}^2}{\epsilon_0\hbar\gamma_2/\gamma_2}$ is the modification of coefficient C in susceptibility χ , and $\Lambda(\Omega_p, \Omega_c, \Omega_s, \Delta_c)$ characterize the resonance as some kind of modified Lorentz profile (see details in Appendix. C). Notably, the Doppler effect can affect resonance profile rather the modification of γ_2 . This may provide the optimal sensing framework for a cold Rydberg-atom-based microwave-field electrometer.

B. Optimal Sensitivity via Fisher Information

Our theoretical framework focuses on optimizing measurement sensitivity through Fisher information maximization. The critical relationship governing this optimization is expressed through the derivative:

$$\frac{\partial F(\Omega_s)}{\partial \Omega_0} = \bar{n}_{tr} \frac{\partial \ln \eta}{\partial \Omega_0} \left[2 \frac{\partial^2 \ln \eta}{\partial \Omega_0^2} + \left(\frac{\partial \ln \eta}{\partial \Omega_0} \right)^2 \right], \quad (23)$$

This enables numerical determination of the optimal reference microwave frequency Ω_0^{opt} . Our approach fundamentally differs from the slope-based optimization method proposed by M. Jing *et al.* [11], which focuses on examination of the transmitted power derivative $k_p = \partial P_{tr}/\partial \Omega_0$ through:

$$\frac{\partial k_p}{\partial \Omega_0} = P_{tr} \frac{\partial \ln \eta}{\partial \Omega_0} \left[\frac{\partial^2 \ln \eta}{\partial \Omega_0^2} + \left(\frac{\partial \ln \eta}{\partial \Omega_0} \right)^2 \right], \quad (24)$$

which have a similar form of Eq. (23).

Figure 2 demonstrates comparative numerical analysis using parameters from Table I. Panel (a) and (c) displays heatmap of Fisher information F_s and transmitted power derivative k_p respectively, using parameters $\Omega_p^{\text{Jing}}/2\pi = 9.3240$ MHz and $\Omega_c^{\text{Jing}}/2\pi = 0.9611$ MHz being calculated from Table I under resonance conditions ($\Delta_s = \Delta_p = 0$) following the work of M. Jing *et al.* [11]. This confirms that three-photon resonance ($\Delta_c = 0$ together with $\Delta_s = \Delta_p = 0$) is the best choice for sensitivity optimization, which is consistent of experimental setup [11]. The dash-dotted vertical line in panels (c-d) indicates the reference microwave frequency $\Omega_0^{\text{Jing}}/2\pi = 7.8964$ MHz from [11], which does not coincide with either the Fisher information maximum ($\Omega_0^{\text{peak}}/2\pi = 10.54633$ MHz) or the k_p extrema ($\Omega_0^{\text{min}}/2\pi = 9.7141$ MHz). This 18.7% relative deviation

($|\Omega_0^{\min} - \Omega_0^{\text{Jing}}|/\Omega_0^{\min}$) suggests significant optimization operable range beyond previous implementations.

The sensitivity comparison in Figure 2(e) reveals progressive improvements: the Jing's scheme yields $\mathcal{E}_s = 1.18 \text{ nV}/(\text{cm}\sqrt{\text{Hz}})$, while slope-optimized and Fisher-optimized approaches achieve $\mathcal{E}_s = 0.94 \text{ nV}/(\text{cm}\sqrt{\text{Hz}})$ and $\mathcal{E}_s = 0.92 \text{ nV}/(\text{cm}\sqrt{\text{Hz}})$, respectively. All theoretical values significantly outperform experimental results ($50 \text{ nV}/(\text{cm}\sqrt{\text{Hz}})$ [11]), with discrepancies attributed to unaccounted technical noise sources and measurement artifacts in practical implementations [35, 36]. These results make our optimization method being reasonable, and their difference in real experimental process is obscured. The working local microwave $\Omega_0/2\pi \sim 10 \text{ MHz}$ in the specific parameter setup can help obtain the optimal sensitivity for experiments.

1. Multiparameter Optimization Analysis

Figure 3(a) presents a 3D parameter space analysis of F_s^{max} versus normalized coupling Rabi frequency ($\Omega_c/\Omega_c^{\text{Jing}}$) and probe-to-coupling ratio (Ω_p/Ω_c). Each surface point represents the maximum F_s for fixed Ω_c, Ω_p over the reference microwave Rabi frequency Ω_0 . Cross-sectional analysis in panel (b) reveals two critical relationships:

- Fixed $\Omega_c = \Omega_c^{\text{Jing}}$: 50% sensitivity improvement through Ω_p/Ω_c optimization ($5 \rightarrow 10$)
- Given ratio $\Omega_p/\Omega_c = 9.7$: Fivefold sensitivity enhancement via Ω_c scaling ($0.5\times \rightarrow 2.5\times$)

Notably, the characteristic inflection point in the fixed-ratio Ω_c dependency curve (dashed blue line) suggests the existence of a critical coupling threshold Ω_c^{crit} beyond which quantum resolution improves dramatically. These results establish fundamental optimization principles for Rydberg electrometer design:

1. Maintain $\Omega_p/\Omega_c \sim 10$ through active laser power stabilization
2. Maximize Ω_c beyond the threshold Ω_c^{crit} within experimental constraints to obtain better sensitivity

The demonstrated parameter dependencies provide practical guidelines for experimental realization of sub- $\text{nV}/(\text{cm}\cdot\sqrt{\text{Hz}})$ sensitivity in Rydberg electrometers.

IV. CONCLUSIONS

In summary, this work presents a comprehensive theoretical analysis of the Fisher information and sensitivity of a Rydberg-atom-based microwave-field electrometer employing the slope detection. Through a detailed examination of the measurement principles and the relationship between Fisher information and sensitivity, we

have provided a quantitative description of the performance of this type of electrometer. The directly measured transmitted probe power is identified as the origin of errors in microwave measurements, as indirectly measured quantities, and this has been verified in this work through two equivalent forms of Fisher information. By considering various non-technical relaxation factors, we have numerically determined the optimal sensing conditions, which provide a theoretical basis for enhancing the performance of the electrometer. Our findings not only contribute to a deeper understanding of the capabilities and limitations of Rydberg-atom-based microwave-field sensing but also lay the groundwork for future applications in the field of precision microwave measurement and sensing technologies.

ACKNOWLEDGMENTS

This work is supported by the Postdoctoral Science Foundation of China under Grants No.2023M733272, and by the Youth Foundation Project of Zhejiang Lab under Grants No.K2023MBOAA04.

Data and code supporting this study are available from the corresponding author upon reasonable request.

Appendix A: The Probe Laser in Coherence state

The optical coherent state is the quantum counterpart of classical light [37]. Consider a monochromatic linearly polarized electromagnetic traveling wave propagating along the \vec{r} -direction. Its quantized electric field component [14] can be expressed as

$$\hat{E}(\vec{r}, t) = i\omega_k \vec{\epsilon}_{\vec{k}s} \left[A_{\vec{k}s} e^{i(\vec{k}\cdot\vec{r} - \omega_k t)} - A_{\vec{k}s}^* e^{-i(\vec{k}\cdot\vec{r} - \omega_k t)} \right], \quad (\text{A1})$$

where

$$A_{\vec{k}s} = \sqrt{\frac{\hbar\omega_k}{2\varepsilon_0 V}} \hat{a},$$

and \hat{a}, \hat{a}^\dagger are the annihilation and creation operator. The electromagnetic wave is obviously time-dependent. However, in the coherent state $|\alpha\rangle$, electromagnetic field can be expressed as

$$\begin{aligned} E(\vec{r}, t) &= \langle \alpha | \hat{E}(\vec{r}, t) | \alpha \rangle \\ &= \omega_k \vec{\epsilon}_{\vec{k}s} \left[\langle \alpha | i A_{\vec{k}s} | \alpha \rangle e^{i(\vec{k}\cdot\vec{r} - \omega_k t)} + h.c. \right] \\ &= \sqrt{\frac{\hbar\omega_k}{2\varepsilon_0 V}} \vec{\epsilon}_{\vec{k}s} \left[i\alpha e^{i(\vec{k}\cdot\vec{r} - \omega_k t)} + h.c. \right] \\ &= \sqrt{\frac{2\hbar\omega_k}{\varepsilon_0 V}} \vec{\epsilon}_{\vec{k}s} |\alpha| \cos(\vec{k}\cdot\vec{r} - \omega_k t + \theta + \pi/2) \quad (\text{A2}) \end{aligned}$$

where $\alpha = |\alpha|e^{i\theta}$, is the parameter of the optical coherent state $|\alpha\rangle$, and it satisfies $\bar{n} = \langle \alpha | \hat{a}^\dagger \hat{a} | \alpha \rangle = |\alpha|^2$. According to the definition, the optical power is the average

energy passing through a certain cross-section per unit time. Therefore,

$$P = \frac{1}{\tau} \left[\frac{1}{\tau} \int_{-\frac{\tau}{2}}^{\frac{\tau}{2}} dt \int \varepsilon_0 |E(\vec{r}, t)|^2 d^3\vec{r} \right] = \frac{\bar{n}\hbar\omega}{\tau} \quad (\text{A3})$$

where $\tau\omega \gg 1$ for a laser, which make sense the sample time τ as discussed in main context. It can be seen that the optical power of electromagnetic wave in coherent state $|\alpha\rangle$ is consistent with the expectation. Electric field components of laser in coherence state thus can be expressed as the expectation of field operator:

$$\begin{aligned} E(\vec{r}, t) &= \langle \alpha | \hat{E}(\vec{r}, t) | \alpha \rangle = E^{(+)}(\vec{r}, t) + E^{(-)}(\vec{r}, t) \\ &= \sqrt{\frac{\hbar\omega_k}{2\varepsilon_0 V}} \vec{\epsilon}_{\vec{k}s} \alpha e^{i(\vec{k}\cdot\vec{r} - \omega_k t + \pi/2)} \\ &\quad + \sqrt{\frac{\hbar\omega_k}{2\varepsilon_0 V}} \vec{\epsilon}_{\vec{k}s} \left[\alpha e^{i(\vec{k}\cdot\vec{r} - \omega_k t + \pi/2)} \right]^*, \end{aligned} \quad (\text{A4})$$

where $E^{(+)}(\vec{r}, t)$ exciting atom from lower energy level to higher one with frequency difference ω , and $E^{(-)}(\vec{r}, t)$ is opposite.

On the other hand, let us consider the probe laser in coherent state propagating through the atom vapor cell as in Fig. (1)(a). When Rational-Wave-Approximation is utilized, one of component can will be irrelevance [14]. For $E^{(+)}(\vec{r}, t)$ part of probe laser or couple laser, two of which are utilized to excite the Rydberg atom to higher energy level. Therefore, when this laser travels trough the atom vapor cell for instance alone the z axis, the $E^{(+)}(\vec{r}, t)$ can be reexpressed as

$$\begin{aligned} E^{(+)}(z, t) &= \sqrt{\frac{\hbar\omega_k}{2\varepsilon_0 V}} \vec{\epsilon}_{k_s} \alpha e^{i(nkz - \omega_k t + \pi/2)} \\ &= \sqrt{\frac{\hbar\omega_k}{2\varepsilon_0 V}} \vec{\epsilon}_{k_s} \alpha e^{i(\text{Re}(n)kz - \omega_k t + \pi/2)} \times e^{-k\text{Im}(n)z}, \end{aligned} \quad (\text{A5})$$

thus, the optical power

$$P(z) = \frac{\hbar\omega}{\tau} \bar{n} e^{-2k\text{Im}(n)z} = P_0 e^{-2k\text{Im}(n)z}, \quad (\text{A6})$$

which recover the laser power relation between the transmitted P_{tr} and incoming $P_{in} = P_0$ when $z = L$ as Fig. (1)(a), and

$$\eta = e^{-2k\text{Im}(n)z},$$

with $n = \sqrt{1 + \chi} \approx 1 + \chi/2$ for weak polarization of atom vapor χ . This is obviously equivalent to a state change from $|\alpha\rangle \rightarrow |\alpha\sqrt{\eta}\rangle$, which just a picture transform from the Schrodinger to Heisenberg picture.

In regard to the laser noise, we should note that the photon emission event is a probabilistic event, while the electron emission event can be described as a stationary random process (memoryless) [37]. The photon emission event of a laser in an optical coherent state follows a

Poisson random process and has a stable photon emission rate denoted as λ (the number of photons emitted per unit time). It can be proved that the number of photons n emitted by a laser in an optical coherent state within the considered time interval τ obeys a Poisson distribution

$$P(n|\lambda\tau) = \frac{(\lambda\tau)^n}{n!} e^{-\lambda\tau} \quad (\text{A7})$$

where, according to the properties of the Poisson distribution, $\bar{n} = \lambda\tau$ is the average number of photons, and the fluctuation of the photon number $\sigma_n = \sqrt{\bar{n}}$. The actual observation process is considered as an N -times independent repeated experimental process (independent and identically distributed) with τ as the inspection time interval (sampling interval), that is, there are N experimental values in chronological order. Considering the power P of photons (the energy of photons flowing through per unit time, analogous to the amount of charge flowing through per unit time), as the observed physical quantity, its sample values in the experiment are P_1, P_2, \dots, P_N , and each power sample $P_i = \frac{\hbar\omega\xi}{\tau}$, where $\xi \sim \pi(\lambda\tau)$ is the power within the sampling interval and also obeys a Poisson distribution. First, it can be determined that the sample mean is

$$\text{E}(P) = \frac{1}{N} \sum_{i=1}^N P_i = \frac{\hbar\omega}{\tau} \text{E}(\xi) = \frac{\hbar\omega}{\tau} \bar{n}. \quad (\text{A8})$$

This is the average power, which is consistent with the above conclusion. The sampling frequency of the random process is $f_s = 1/\tau$. According to the Nyquist sampling theorem [38], the bandwidth of the random experiment can be correspondingly defined as

$$B = \frac{f_s}{2} = \frac{1}{2\tau}. \quad (\text{A9})$$

In this way, the fluctuation of the power can be considered. First, consider the power fluctuation

$$\begin{aligned} [\sigma_P]_n &= \sqrt{\frac{2\tau}{N} \sum_{i=1}^N [P_i - \text{E}(P)]^2} \\ &= \sqrt{2\tau \text{E} \left(\left[\frac{\hbar\omega}{\tau} \xi - \text{E}(P) \right]^2 \right)} \\ &= \sqrt{2\tau \left(\frac{\hbar\omega}{\tau} \right)^2 \text{Var}(\xi)} \\ &= \sqrt{2\tau \left(\frac{\hbar\omega}{\tau} \right)^2 \text{E}(\xi)} \\ &= \sqrt{2\hbar\omega \text{E}(P)}. \end{aligned} \quad (\text{A10})$$

Compared with the expression of the root mean square power

$$[\sigma_P]_{\text{rms}} = \sqrt{\frac{1}{N} \sum_{i=1}^N [P_i - \text{E}(P)]^2}, \quad (\text{A11})$$

which is in essence the fluctuation of laser power, it takes the sampling time into account. From the relationship between them

$$[\sigma_P]_n = \frac{[\sigma_P]_{\text{rms}}}{\sqrt{B}} \quad (\text{A12})$$

it can be seen that the root mean square power $[\sigma_P]_{\text{rms}}$ is the theoretical total power spectrum, while the power fluctuation $[\sigma_P]_n$ represents the total power spectrum within a unit bandwidth, that is, the power spectral density. They have different dimensions, and the source of the difference comes from the finite sampling rate $f_s = 1/\tau$ of the random experiment, that is, the measurement process of light. In general engineering practice, the power spectral density is used to measure the size of the noise because the measurement result should not depend on the measurement process and instrument. At the same time, the power spectral density and the autocorrelation function of the power are a pair of Fourier transforms, which has a clear physical meaning in spectral analysis.

Appendix B: Fisher Information From Parameter Estimation

The Cramér-Rao inequality [10, 28] in parameter estimation claims that the measurement error of the microwave to be measured as a parameter to be estimated will not be infinitesimal but has a lower bound

$$\Delta\Omega_s = \sqrt{\text{Var}[\Omega_s]} \geq \frac{\left| \frac{\partial P_{tr}}{\partial \Omega_0} \right|}{\sqrt{F(\Omega_s)}}, \quad (\text{B1})$$

where $F(\Omega_s)$ is the Fisher information. Following the parameter estimation theory, the definition of Fisher information [28] to estimate the parameter θ is

$$F(\theta) = \int p(x|\theta) \left[\frac{\partial \ln p(x|\theta)}{\partial \theta} \right]^2 dx. \quad (\text{B2})$$

The likelihood function for the Rydberg-atom-based electrometer is, in turn, the Poisson distribution of photon numbers, which is approximately Gaussian for large photon numbers, i.e.,

$$p(n|\Omega_s) = \frac{1}{\sqrt{2\pi\bar{n}_{tr}}} \exp \left[-\frac{(n - \bar{n}_{tr})^2}{2\bar{n}_{tr}} \right], \quad (\text{B3})$$

where $\sigma_{n_{tr}} = \sqrt{\bar{n}_{tr}}$ and $\bar{n}_{tr} = \bar{n}_0\eta(\Omega_s)$ in Eq. (2). We thus can easily solve the Fisher information through some mathematical calculations as

$$\begin{aligned} F_{\text{def}}(\Omega_s) &= \left(\frac{\partial \bar{n}_{tr}}{\partial \Omega_0} \right)^2 \int p(n|\Omega_s) \left[\frac{\partial \ln p(n|\Omega_s)}{\partial \bar{n}_{tr}} \right]^2 dn \\ &= \frac{1}{\bar{n}_{tr}} \left(\frac{\partial \bar{n}_{tr}}{\partial \Omega_0} \right)^2 = \bar{n}_{tr} \left(\frac{\partial \ln \eta}{\partial \Omega_0} \right)^2 \end{aligned} \quad (\text{B4})$$

taking into account the general Gaussian integral and the substantial average photon numbers \bar{n}_{tr} emitted by the probe laser in time τ . It follows that:

$$\int p(n|\Omega_s) \left[\frac{\partial \ln p(n|\Omega_s)}{\partial \bar{n}_{tr}} \right]^2 dn = \frac{1 + 2\bar{n}_{tr}}{2\bar{n}_{tr}^2} \approx \frac{1}{\bar{n}_{tr}}, \quad (\text{B5})$$

where the last \approx is obvious since $\bar{n}_{tr} \gg 1$. Consequently, we acquire the quantitative characterization of the accuracy limit for microwave electric measurement around the reference microwave Ω_L in two equivalent forms of manifestations. This actually, in some sense, checks our analysis of errors on which the Fisher information depends to tell the limit of measurement precision.

Appendix C: Relaxations and Master Equation

1. The Decay Relaxation

□ spontaneous emission

As mentioned above, the vacuum fluctuations of the electromagnetic field lead to the spontaneous emission of atomic energy levels. The spontaneous emission transition rate of the atomic energy level $J_e \rightarrow J_g$ is [14]

$$\Gamma_{F_e F_g} \approx \Gamma_{J_e J_g} = \frac{e^2 \omega_{J_e \rightarrow J_g}^3}{3\pi \epsilon_0 \hbar c^3} \frac{2J_g + 1}{2J_e + 1} |\langle J_g || r || J_e \rangle|^2 \quad (\text{C1})$$

The decay rate of the atomic energy level due to spontaneous emission should [15] consider summing over the lower energy states to represent the spontaneous emission decay rate of the atom in the $n_e L_e J_e$ state as

$$\Gamma_0 = \sum_{E_{n_g L_g J_g} < E_{n_e L_e J_e}} \Gamma_{n_g L_g J_g, n_e L_e J_e}. \quad (\text{C2})$$

□ thermal radiation

The thermal radiation from the environment at a finite temperature will lead to the stimulated emission and stimulated absorption of atoms. Therefore, for the transition of $J_e \rightarrow J_g$, the transition rates of stimulated emission and stimulated absorption are determined by the Einstein B coefficient and the spectral energy density of thermal radiation, satisfying the Planck blackbody radiation law

$$\rho(\omega) d\omega = \frac{\mathcal{D}(\hbar\omega)}{\exp\left(\frac{\hbar\omega}{k_B T}\right) - 1} d\omega, \quad (\text{C3})$$

where the mode density [14, 39] of the spatial electromagnetic wave

$$\mathcal{D}(\omega) = \frac{\omega^2}{\pi^2 c^3}, \quad (\text{C4})$$

and thus the energy density are

$$\mathcal{D}(\hbar\omega) = \hbar\omega\mathcal{D}(\omega) = \frac{\hbar\omega^3}{\pi^2c^3}.$$

So the transition rates of stimulated emission and stimulated absorption can both be expressed as [15]

$$W_{J_gJ_e} = B_{ba} \frac{\mathcal{D}(\hbar\omega_{J_e \rightarrow J_g})}{\exp\left(\frac{\hbar\omega_{J_e \rightarrow J_g}}{k_B T}\right) - 1} = \frac{\Gamma_{J_eJ_g}}{\exp\left(\frac{\hbar\omega_{J_e \rightarrow J_g}}{k_B T}\right) - 1} \quad (\text{C5})$$

with $A_{ba} = B_{ba}\mathcal{D}(\hbar\omega)$ [40]. The spectral coverage of thermal radiation is $\omega \in [0, \infty)$. Therefore, the rate of change of the atomic energy level population due to thermal radiation [15] should sum over all the allowed atomic energy states

$$\Gamma_{BBR} = \sum_{E_{n_gL_gJ_g}} W_{n_gL_gJ_g, n_eL_eJ_e} \quad (\text{C6})$$

which represents the decay rate of the atom in the $n_eL_eJ_e$ state due to thermal radiation. The sponta-

neous emission and thermal radiation together determine the decay rate

$$\gamma = \Gamma_0 + \Gamma_{BBR}$$

of the atomic energy state in the atomic ensemble. Therefore, for the selected 4-level structure of the ^{133}Cs atom

$$\begin{aligned} |1\rangle &= |6^2S_{1/2}(F=4)\rangle, |2\rangle = |6^2P_{3/2}(F'=5)\rangle \\ |3\rangle &= |47^2D_{5/2}\rangle, |4\rangle = |48^2P_{3/2}\rangle \end{aligned}$$

the effective decay rates of all three excited energy levels can be calculated (using the getStateLifetime function in the RAC Python package [15]) as in Tab. I. Therefore, the atomic decay involves the transitions of $|2\rangle \rightarrow |1\rangle$, $|3\rangle \rightarrow |2\rangle$, $|4\rangle \rightarrow |1\rangle$. It is noted that the direct transition of $|3\rangle \rightarrow |1\rangle$ is forbidden. In the case of spontaneous emission and thermal radiation, the atomic state $|3\rangle$ can only decay to $|2\rangle$. Therefore, the decay process is $|3\rangle \rightarrow |2\rangle$ rather than $|3\rangle \rightarrow |1\rangle$. The decay dissipation term [11, 34] for the selected hot Cs atomic ensemble can be determined as

$$\mathcal{L}_{decay}\tilde{\rho} = \begin{bmatrix} \gamma_2\rho_{22} + \gamma_4\rho_{44} & -\frac{\gamma_2}{2}\rho_{12} & -\frac{\gamma_3}{2}\rho_{13} & -\frac{\gamma_4}{2}\rho_{14} \\ -\frac{\gamma_2}{2}\rho_{21} & \gamma_3\rho_{33} - \gamma_2\rho_{22} & -\frac{\gamma_2+\gamma_3}{2}\rho_{23} & -\frac{\gamma_2+\gamma_4}{2}\rho_{24} \\ -\frac{\gamma_3}{2}\rho_{31} & -\frac{\gamma_3+\gamma_2}{2}\rho_{32} & -\gamma_3\rho_{33} & -\frac{\gamma_3+\gamma_4}{2}\rho_{34} \\ -\frac{\gamma_4}{2}\rho_{41} & -\frac{\gamma_4+\gamma_2}{2}\rho_{42} & -\frac{\gamma_4+\gamma_3}{2}\rho_{43} & -\gamma_4\rho_{44} \end{bmatrix}. \quad (\text{C7})$$

2. The Dephasing Relaxation

□ atom-atom collision

In the vapor cell, the ^{133}Cs atoms have three states, namely the Rydberg state (R), Intermediate state (M), and Ground state (G) under the interaction with the laser. The collisions between atoms can occur in six ways: R-R, R-M, R-G, M-M, M-G, and G-G, and each type of collision can be further divided into elastic and inelastic collisions. However, the R-G collision is the main contribution to the collision broadening of Rydberg atoms [19, 20, 22]. And in the absence of impurity atoms, the collision dephasing rate between the Rydberg state with the principal quantum number $n > 30$ [41] and the ground state atoms is

$$\Gamma_c = \mathcal{N}_0\bar{v}\sigma(v, C_s) = \Gamma_{c,el} + \Gamma_{c,in}, \quad (\text{C8})$$

where the inelastic collision can be expressed in the International System of Units as

$$\Gamma_{c,in} = \frac{8e^2a_s^2}{4\pi\epsilon_0\hbar n^*}\mathcal{N}_0$$

$$= \frac{1.352 \times 10^{-11}}{n^*} \text{Hz} \cdot \text{m}^3 \times \mathcal{N}_0, \quad (\text{C9})$$

and the elastic collision at room temperature can be expressed in the International System of Units as

$$\begin{aligned} \Gamma_{c,el} &= 7.18 \left[\left(\frac{\alpha c}{4\pi\epsilon_0} \mathcal{A} \right)^2 \bar{v} \right]^{1/3} \mathcal{N}_0 \\ &= 1.111 \times 10^{-13} \text{Hz} \cdot \text{m}^3 \times \mathcal{N}_0, \end{aligned} \quad (\text{C10})$$

Here, \mathcal{N}_0 is the density of ground state atoms, and \mathcal{A} is the atomic ground state polarizability in International System of Units

$$\mathcal{A} = \beta_{\mathcal{A}}\mathcal{A}_a = 4\pi\epsilon_0 a_0^3 \mathcal{A}_a,$$

where $\mathcal{A}_{Cs,a} = 402.2$ is that the ^{133}Cs atom in the Hartree atomic unit where system $\beta_{\mathcal{A}} = 4\pi\epsilon_0 a_0^3$ [42, 43]. \bar{v} is the average velocity of vapor atoms under the Boltzmann distribution

$$\bar{v} = \sqrt{\frac{8k_B T}{\pi m_{Cs}}},$$

with the mass of the Cs atom is

$$m_{Cs} = 132.90545196u$$

with atom mass unit $u = 1.6605390666 \times 10^{-27}$ kg. Additionally, $a_s = -16.6075a_0$ is the average s-wave scattering length of the singlet and triplet scattering channels of the Cs atom (by $\frac{1}{4}$ singlet + $\frac{3}{4}$ triplet) [44], and $n^* = n - \delta_{nlj}$ is the effective quantum number of the Rydberg state with quantum defect δ_{nlj} . Thus, these collision parameters can all be calculated by the ARC package [15]. In addition, the saturated vapor of ^{133}Cs atoms in the vapor cell The dependence of the vapor pressure on temperature satisfies [14]:

$$\log_{10} \frac{P_v}{133.322368} = 2.881 + 4.711 - \frac{3999}{T}.$$

Based on the gas state equation $P_v = \mathcal{N}_0 k_B T$, the atomic number density $N_0 = N/V$ can thus be determined. Given the ambient temperature is $T = 298.15$ K, the atomic number density can be calculated as $\mathcal{N}_0 = 2.93910^{16} \text{ m}^{-3}$. Therefore, the collision broadening

$$\Gamma_{c,in} = \frac{661.546}{n^*} \text{ kHz} = \begin{cases} 8.921, & n = 47 \\ 8.940, & n = 48 \end{cases},$$

$$\Gamma_{c,el} = 3.256 \text{ kHz}.$$

Therefore, $\Gamma_{c3} = 8.921 + 3.256 = 1.938 \times 2\pi \text{ kHz}$, $\Gamma_{c4} = 8.940 + 3.256 = 1.941 \times 2\pi \text{ kHz}$. It can be seen that the collision broadening effect is on the order of 10 kHz, which is comparable to the decay rate of the Cs atom Rydberg states $|47D_{5/2}\rangle$ and $|48P_{3/2}\rangle$. Thus, the dephasing process caused by the collision only involves $|3\rangle \rightarrow |1\rangle$, $|4\rangle \rightarrow |1\rangle$. The corresponding Lindblad relaxation term [34] can be determined as

$$\mathcal{L}_{col}\tilde{\rho} = \begin{bmatrix} 0 & 0 & -\Gamma_{c3}\rho_{13} & -\Gamma_{c4}\rho_{14} \\ 0 & 0 & 0 & 0 \\ -\Gamma_{c3}\rho_{31} & 0 & 0 & 0 \\ -\Gamma_{c4}\rho_{41} & 0 & 0 & 0 \end{bmatrix}. \quad (\text{C11})$$

□ laser linewidth

The energy spectral density of the laser [20] has a Voigt profile. For the convenience of explanation, assume it has a Lorentzian profile. Frequencies other than those resonant with the atoms in energy spectral density will cause non-resonant transitions of other atoms in the atomic ensemble, resulting in the dephasing of the atomic ensemble excitation. Assume that the probe light and the coupling light are independent of each other. The dephasing processes include $|1\rangle \leftrightarrow |2\rangle$ caused by the linewidth γ_p of the probe light and $|2\rangle \leftrightarrow |3\rangle$ caused by the linewidth γ_c of the coupling light. Then the corresponding Lindblad relaxation terms [34, 45] can be determined as

$$\mathcal{L}_{lw}\tilde{\rho} = \begin{bmatrix} 0 & -\gamma_p\rho_{12} & -(\gamma_p + \gamma_c)\rho_{13} & -(\gamma_p + \gamma_c)\rho_{14} \\ -\gamma_p\rho_{21} & 0 & -\gamma_c\rho_{23} & -\gamma_c\rho_{24} \\ -(\gamma_p + \gamma_c)\rho_{31} & -\gamma_c\rho_{32} & 0 & 0 \\ -(\gamma_p + \gamma_c)\rho_{41} & -\gamma_c\rho_{42} & 0 & 0 \end{bmatrix}. \quad (\text{C12})$$

Since the probe light and the coupling light are independent of each other and assuming the microwave linewidth is zero, both $|1\rangle \leftrightarrow |3\rangle$ and $|1\rangle \leftrightarrow |4\rangle$ are caused by both the probe and the coupling, and the sum of the linewidths is $\gamma_p + \gamma_c$. The typical linewidth of a laser is usually several hundred kHz [19, 20, 33], which is much larger than the spontaneous emission, black-body radiation, and collision broadening. However, the laser linewidth can also be narrowed by various frequency-stabilization methods. Currently, it is possible to achieve frequency-stabilization to the order of $\gamma \sim \text{mHz}$ or even smaller [11, 29–32]. Using such a narrow-linewidth laser, whose linewidth is much smaller than the natural linewidth of the atomic energy level, we do not need to consider the dephasing effect of the laser linewidth.

□ transit-time

The transit time of atom transversely traveling through the finite width of laser beam lead to frequency spreading. Atoms move in the direction perpendicular to the light propagation. Due to the finite radius of the laser beam, atoms will pass through the spot ranges of the probe light and the couple light within a finite time. What atoms feel are two light pulses rather than a continuous wave, resulting in frequency spreading near the continuous wave frequency. Such a relaxation process is called transit-time relaxation, which is similar to atomic collisions, leading to the dephasing of the energy levels of the atomic ensemble [17, 18]. The transit-induced energy level broadening is

$$\Gamma_t = 1.33 \frac{v_{\text{rms}}}{w_0}, \quad (\text{C13})$$

where

$$v_{\text{rms}} = \sqrt{\frac{2k_B T}{m_{Cs}}}$$

is the two-dimensional root mean square velocity. The transit relaxation rate Γ_t is inversely proportional to the waist radius w_0 of the laser. It can be estimated that for a laser with a waist radius on the order of mm at room temperature, the transit relaxation rate $\Gamma_t \approx 0.3$ kHz, which is much smaller than the collision relaxation rate. Therefore, increasing the waist radii of the probe light and the couple light can greatly suppress the transit relaxation [11], so that the influence of the transit relaxation will not be considered.

□ laser power broadening

The probe laser power broaden the atom transition rate, but can be embedded into the master equation solve, so we do not explain and the details can be seen in Ref. ([14]).

□ The Hanle effect

induced by weak earth magnetic field can in principle not be ignored, which results in observable optical effect using polarized excitation laser. But we only concentrate on the uncontrollable relaxation, in this sense, the earth magnetic field can be conceal by magnetic compensation and will be not considered here too.

□ Doppler effect

The Doppler effect is manifested as the frequency shift caused by the motion of atoms along the direction of light propagation, and it appears as spectral line broadening after ensemble averaging. Firstly, assume that the light propagates along the z-direction. For an atom moving in the z-direction, the frequency of the absorbed photon is

$$\omega = \omega_{s0} - \vec{k} \cdot \vec{v} = \omega_{s0} \left(1 - \frac{v_z}{c}\right). \quad (\text{C14})$$

If it moves in the opposite direction, the sign changes. Similarly, when an atom moves towards the photon detector and emits a photon, the received frequency is

$$\omega = \omega_{e0} \left(1 + \frac{v_z}{c}\right).$$

Whether it is absorption or emission, the frequency shifts due to the motion of the atom. Now consider the Doppler broadening effect of atomic spontaneous emission. For a one-dimensional Boltzmann distribution

$$w(v) = \frac{1}{\sqrt{2\pi}v_{th}} \exp\left(-\frac{v^2}{2v_{th}^2}\right), \quad (\text{C15})$$

where

$$v_{th} = \sqrt{\frac{k_B T}{m_{Cs}}}$$

is the most probable speed of the one-dimensional random thermal motion of Cs atoms. The atomic number density with a velocity component in the range $[v_z, v_z + dv_z]$ per unit volume is

$$n(v_z)dv_z = \mathcal{N}_0 w(v_z)dv_z$$

where \mathcal{N}_0 is the Cs atomic number density. Then, due to the motion of the atom, the atomic number density of photons with a received frequency in the range $[\omega, \omega + d\omega]$ can be determined as

$$n(\omega)d\omega = \frac{\mathcal{N}_0}{\sqrt{2\pi}\omega_{th}} \exp\left[-\frac{(\omega - \omega_{e0})^2}{2\omega_{th}^2}\right] d\omega, \quad (\text{C16})$$

where

$$\omega_{th} = \frac{v_{th}}{c}\omega_{e0} = \frac{\omega_{e0}}{c} \sqrt{\frac{k_B T}{m_{Cs}}}.$$

The received light intensity $I(\omega)d\omega \propto n(\omega)d\omega$, and the received light intensity spectral density is

$$I(\omega) = I_0 \exp\left[-\frac{(\omega - \omega_{e0})^2}{2\omega_{th}^2}\right], \quad (\text{C17})$$

where I_0 is the frequency density of the atomic spontaneous emission light intensity and has a Lorentzian line shape

$$I_0 \propto \frac{\gamma/2\pi}{(\omega - \omega_{e0})^2 + (\frac{\gamma}{2})^2}. \quad (\text{C18})$$

Therefore, the total light intensity

$$I \propto \int_0^\infty \frac{\gamma/2\pi}{(\omega - \omega_{e0})^2 + (\frac{\gamma}{2})^2} \exp\left[-\frac{(\omega - \omega_{e0})^2}{2\omega_{th}^2}\right] d\omega \quad (\text{C19})$$

This is the Voigt lineshape. It is easy to obtain the full width at half maximum of the Doppler effect

$$\gamma_D = \omega - \omega_{e0} = \sqrt{2 \ln 2} \omega_{th} = \frac{\omega_{e0}}{c} \sqrt{\frac{2 \ln 2 k_B T}{m_{Cs}}}. \quad (\text{C20})$$

It can be calculated that this Doppler width is basically in the order of several hundred MHz, which is much larger than the natural linewidth of the energy level.

Based on the above, we include decay relaxation due to spontaneous emission and environmental thermal radiation, as well as non-technical dephasing relaxation factors such as atomic collision broadening, Doppler broadening, and laser power broadening. We intend not to consider technical controllable dephasing relaxation like laser linewidth, transit time, and magnetic field Hanle effect, as stated in the main text. Consequently, the Lindblad dissipation term in the master equation [Eq. (16)] is determined from spontaneous emission, thermal radiation, and atomic collisions as:

$$\begin{aligned}
\mathcal{L}\tilde{\rho} &= \mathcal{L}_{decay}\tilde{\rho} + \mathcal{L}_{deph}\tilde{\rho} \\
&= \begin{bmatrix} \gamma_2\rho_{22} + \gamma_4\rho_{44} & -\frac{\gamma_2}{2}\rho_{12} & -\left(\frac{\gamma_3}{2} + \Gamma_{c3}\right)\rho_{13} & -\left(\frac{\gamma_4}{2} + \Gamma_{c4}\right)\rho_{14} \\ -\frac{\gamma_2}{2}\rho_{21} & \gamma_3\rho_{33} - \gamma_2\rho_{22} & -\frac{\gamma_2+\gamma_3}{2}\rho_{23} & -\frac{\gamma_2+\gamma_4}{2}\rho_{24} \\ -\left(\frac{\gamma_3}{2} + \Gamma_{c3}\right)\rho_{31} & -\frac{\gamma_3+\gamma_2}{2}\rho_{32} & -\gamma_3\rho_{33} & -\frac{\gamma_3+\gamma_4}{2}\rho_{34} \\ -\left(\frac{\gamma_4}{2} + \Gamma_{c4}\right)\rho_{41} & -\frac{\gamma_4+\gamma_2}{2}\rho_{42} & -\frac{\gamma_4+\gamma_3}{2}\rho_{43} & -\gamma_4\rho_{44} \end{bmatrix} \\
&= \begin{bmatrix} \gamma_2\rho_{22} + \gamma_4\rho_{44} & -\gamma_{21}\rho_{12} & -\gamma_{31}\rho_{13} & -\gamma_{41}\rho_{14} \\ -\gamma_{21}\rho_{21} & \gamma_3\rho_{33} - \gamma_2\rho_{22} & -\gamma_{32}\rho_{23} & -\gamma_{42}\rho_{24} \\ -\gamma_{31}\rho_{31} & -\gamma_{32}\rho_{32} & -\gamma_3\rho_{33} & -\gamma_{43}\rho_{34} \\ -\gamma_{41}\rho_{41} & -\gamma_{42}\rho_{42} & -\gamma_{43}\rho_{43} & -\gamma_4\rho_{44} \end{bmatrix}, \tag{C21}
\end{aligned}$$

where

$$\begin{aligned}
\gamma_{12} &= \gamma_{21} = \frac{\gamma_2}{2}, \\
\gamma_{13} &= \gamma_{31} = \frac{\gamma_3}{2} + \Gamma_{c3}, \\
\gamma_{14} &= \gamma_{41} = \frac{\gamma_4}{2} + \Gamma_{c4}, \\
\gamma_{23} &= \gamma_{32} = \frac{\gamma_3 + \gamma_2}{2}, \\
\gamma_{24} &= \gamma_{42} = \frac{\gamma_2 + \gamma_4}{2}, \\
\gamma_{34} &= \gamma_{43} = \frac{\gamma_3 + \gamma_4}{2}.
\end{aligned}$$

With this, the master equation can be obtained, and the Doppler effect will be carried out by the average of density matrix solution over Boltzmann distribution.

3. Calculation Details

In this way, the system master equation can be determined as $AX = b$, as

$$\begin{aligned}
0 &= -2\gamma_2\rho_{22} - 2\gamma_4\rho_{44} - i\Omega_p(\tilde{\rho}_{12} - \tilde{\rho}_{21}) \\
0 &= -2(\gamma_{21} + i\Delta_p)\tilde{\rho}_{12} + i\Omega_c\tilde{\rho}_{13} + i\Omega_p(\rho_{11} - \rho_{22}) \\
0 &= -2[\gamma_{31} + i(\Delta_p + \Delta_c)]\tilde{\rho}_{13} + i\Omega_c\tilde{\rho}_{12} + i\Omega_0\tilde{\rho}_{14} - i\Omega_p\tilde{\rho}_{23} \\
0 &= -2[\gamma_{41} + i(\Delta_p + \Delta_c - \Delta_L)]\tilde{\rho}_{14} + i\Omega_0\tilde{\rho}_{13} - i\Omega_p\tilde{\rho}_{24} \\
0 &= -2(\gamma_{21} - i\Delta_p)\tilde{\rho}_{21} - i\Omega_c\tilde{\rho}_{31} - i\Omega_p(\rho_{11} - \rho_{22}) \\
0 &= -2\gamma_2\rho_{22} + 2\gamma_3\rho_{33} + i\Omega_c(\tilde{\rho}_{23} - \tilde{\rho}_{32}) - i\Omega_p(\tilde{\rho}_{12} - \tilde{\rho}_{21}) \\
0 &= -2(\gamma_{32} + i\Delta_c)\tilde{\rho}_{23} + i\Omega_c(\rho_{22} - \rho_{33}) + i\Omega_0\tilde{\rho}_{24} - i\Omega_p\tilde{\rho}_{13} \\
0 &= -2[\gamma_{42} + i(\Delta_c - \Delta_L)]\tilde{\rho}_{24} - i\Omega_c\tilde{\rho}_{34} + i\Omega_0\tilde{\rho}_{23} - i\Omega_p\tilde{\rho}_{14} \\
0 &= -2[\gamma_{31} - i(\Delta_p + \Delta_c)]\tilde{\rho}_{31} - i\Omega_c\tilde{\rho}_{21} - i\Omega_0\tilde{\rho}_{41} + i\Omega_p\tilde{\rho}_{32} \\
0 &= -2[\gamma_{32} - i\Delta_c]\tilde{\rho}_{32} - i\Omega_c(\rho_{22} - \rho_{33}) - i\Omega_0\tilde{\rho}_{42} + i\Omega_p\tilde{\rho}_{31} \\
0 &= -2\gamma_3\rho_{33} - i\Omega_c(\tilde{\rho}_{23} - \tilde{\rho}_{32}) + i\Omega_0(\tilde{\rho}_{34} - \tilde{\rho}_{43}) \\
0 &= -2(\gamma_{43} - i\Delta_L)\tilde{\rho}_{34} - i\Omega_c\tilde{\rho}_{24} + i\Omega_0(\rho_{33} - \rho_{44}) \\
0 &= -2[\gamma_{41} - i(\Delta_p + \Delta_c - \Delta_L)]\tilde{\rho}_{41} - i\Omega_0\tilde{\rho}_{31} + i\Omega_p\tilde{\rho}_{42} \\
0 &= -2[\gamma_{42} - i(\Delta_c - \Delta_L)]\tilde{\rho}_{42} + i\Omega_c\tilde{\rho}_{43} - i\Omega_0\tilde{\rho}_{32} + i\Omega_p\tilde{\rho}_{41} \\
0 &= -2(\gamma_{43} + i\Delta_L)\tilde{\rho}_{43} + i\Omega_c\tilde{\rho}_{42} - i\Omega_0(\rho_{33} - \rho_{44}) \\
0 &= -2\gamma_4\rho_{44} - i\Omega_0(\tilde{\rho}_{34} - \tilde{\rho}_{43})
\end{aligned}$$

$$1 = \rho_{11} + \rho_{22} + \rho_{33} + \rho_{44}$$

where $\tilde{\rho}_{12} = \rho_{12}e^{i\omega_p t}$, $\tilde{\rho}_{23} = \rho_{32}e^{i\omega_c t}$, $\tilde{\rho}_{34} = \rho_{34}e^{i\Omega_0 t}$ and $\rho_{ij}^* = \rho_{ji}$. Thereby, the steady state condition $\partial\tilde{\rho}/\partial t = 0$ and the probability normalization condition $\text{tr}[\tilde{\rho}] = 1$ is

used. Noting that coefficient A is a full column rank matrix, thus, satisfies

$$X = A^{-1}b = (A^\dagger A)^{-1}A^\dagger b, \tag{C22a}$$

$$\begin{aligned}
\frac{\partial X}{\partial \Omega_s} &= -A^{-1}\frac{\partial A}{\partial \Omega_s}A^{-1}b \\
&= -(A^\dagger A)^{-1}A^\dagger\frac{\partial A}{\partial \Omega_s}(A^\dagger A)^{-1}A^\dagger b \tag{C22b}
\end{aligned}$$

The Doppler effect of random moving atom when absorbing or emitting light can be incorporated into the solution of $AX = b$ by average,

$$D[X(\Delta'_p, \Delta'_c)] = \int_{-\infty}^{\infty} X(\Delta'_p, \Delta'_c)w(v)dv, \tag{C23}$$

where

$$\Delta'_p = \Delta_p + \frac{2\pi}{\lambda_p}v, \Delta'_c = \Delta_c - \frac{2\pi}{\lambda_c}v,$$

with the one-dimensional Boltzmann distribution

$$w(v) = \frac{1}{\sqrt{2\pi}v_{th}} \exp\left(-\frac{v^2}{2v_{th}^2}\right).$$

Thus, we can completely carry out the slope maximum microwave before Doppler average which lead to no difference for the Doppler average results. The laser power broadening effect has been included in the equations. We will first solve for the density matrix and then consider the correction of the Doppler broadening effect on the density matrix. The above constitutes a set of linear equations with 16 independent parameters, and it is almost impossible to solve them analytically, so numerical solutions are required. This can be solved numerically. The atomic thermal noise corrects the attenuation coefficient (polarizability χ) of the probe light passing through the atomic vapor cell, and finally the thermal motion broadening effect of the atom is represented by the final effective attenuation coefficient

$$\eta = \exp\left\{-\frac{2\pi L}{\lambda_p} \text{Im}(D[\chi])\right\}, \tag{C24}$$

where χ is the susceptibility of atom vapor, and $D[\chi]$ its Doppler transformation. This expression provides the desired basis for numerical analysis.

- [1] C. S. Adams, J. D. Pritchard, and J. P. Shaffer, Rydberg atom quantum technologies, *Journal of Physics B: Atomic, Molecular and Optical Physics* **53**, 012002 (2019).
- [2] A. Artusio-Glimpse, M. T. Simons, N. Prajapati, and C. L. Holloway, Modern RF measurements with hot atoms: A technology review of rydberg atom-based radio frequency field sensors, *IEEE Microw. Mag.* **23**, 44 (2022).
- [3] J. A. Sedlacek, A. Schwettmann, H. Kübler, R. Löw, T. Pfau, and J. P. Shaffer, Microwave electrometry with Rydberg atoms in a vapour cell using bright atomic resonances, *Nature Physics* **8**, 819 (2012).
- [4] J. A. Sedlacek, A. Schwettmann, H. Kübler, and J. P. Shaffer, Atom-based vector microwave electrometry using Rubidium Rydberg atoms in a vapor cell, *Physical Review Letters* **111**, 063001 (2013).
- [5] C. L. Holloway, J. A. Gordon, S. Jefferts, A. Schwarzkopf, D. A. Anderson, S. A. Miller, N. Thaicharoen, and G. Raithel, Broadband Rydberg atom-based electric-field probe for SI-traceable, self-calibrated measurements, *IEEE Transactions on Antennas and Propagation* **62**, 6169 (2014).
- [6] H. Fan, S. Kumar, J. Sedlacek, H. Kübler, S. Karimkashi, and J. P. Shaffer, Atom based RF electric field sensing, *Journal of Physics B: Atomic, Molecular and Optical Physics* **48**, 202001 (2015).
- [7] M. T. Simons, A. H. Haddab, J. A. Gordon, and C. L. Holloway, A Rydberg atom-based mixer: Measuring the phase of a radio frequency wave, *Applied Physics Letters* **114** (2019).
- [8] A. K. Robinson, N. Prajapati, D. Senic, M. T. Simons, and C. L. Holloway, Determining the angle-of-arrival of a radio-frequency source with a Rydberg atom-based sensor, *Applied Physics Letters* **118** (2021).
- [9] J. Hu, H. Li, R. Song, J. Bai, Y. Jiao, J. Zhao, and S. Jia, Continuously tunable radio frequency electrometry with Rydberg atoms, *Applied Physics Letters* **121** (2022).
- [10] C. L. Degen, F. Reinhard, and P. Cappellaro, Quantum sensing, *Reviews of Modern Physics* **89**, 035002 (2017).
- [11] M. Jing, Y. Hu, J. Ma, H. Zhang, L. Zhang, L. Xiao, and S. Jia, Atomic superheterodyne receiver based on microwave-dressed Rydberg spectroscopy, *Nature Physics* **16**, 911 (2020).
- [12] S. L. Braunstein and C. M. Caves, Statistical distance and the geometry of quantum states, *Physical Review Letters* **72**, 3439 (1994).
- [13] D. Spehner and M. Orszag, Geometric quantum discord with bures distance, *New Journal of Physics* **15**, 103001 (2013).
- [14] D. A. Steck, Quantum and atom optics, Website (2024), <http://steck.us/teaching>.
- [15] N. Šibalić, J. D. Pritchard, C. S. Adams, and K. J. Weatherill, ARC: An open-source library for calculating properties of alkali rydberg atoms, *Computer Physics Communications* **220**, 319 (2017).
- [16] A. Omont, On the theory of collisions of atoms in rydberg states with neutral particles, *Journal de Physique* **38**, 1343 (1977).
- [17] J. Sagle, R. Namiotka, and J. Huennekens, Measurement and modelling of intensity dependent absorption and transit relaxation on the cesium line, *Journal of Physics B: Atomic, Molecular and Optical Physics* **29**, 2629 (1996).
- [18] Q. Fontaine, *Paraxial fluid of light in hot atomic vapors*, Theses, Sorbonne Université (2020).
- [19] S. Kumar, H. Q. Fan, H. Kübler, J. Sheng, and J. P. Shaffer, Atom-based sensing of weak radio frequency electric fields using homodyne readout, *Scientific Reports* **7**, 42981 (2016).
- [20] J. S. Otto, N. Kjærgaard, and A. B. Deb, *Towards Quantum Information Processing with Rydberg Atoms in an Interspecies K-Rb System*, Ph.D. thesis, University of Otago (2022).
- [21] R. Finkelstein, S. Bali, O. Firstenberg, and I. Novikova, A practical guide to electromagnetically induced transparency in atomic vapor, *New Journal of Physics* **25**, 035001 (2023).
- [22] H. Fan, *Microwave Electrometry with Rydberg Electromagnetically Induced Transparency in Vapor Cells*, Ph.D. thesis, University of Oklahoma (2015).
- [23] D. A. Steck, Cesium d line data, Website (2024), <https://steck.us/alkalidata/cesiumnumbers.pdf>.
- [24] N. Prajapati, N. Bhusal, A. P. Rotunno, S. Berweger, M. T. Simons, A. B. Artusio-Glimpse, Y. Ju Wang, E. Bottomley, H. Fan, and C. L. Holloway, Sensitivity comparison of two-photon vs three-photon rydberg electrometry, *Journal of Applied Physics* **134** (2023).
- [25] J. R. Venneberg, *Measurement and reduction of laser power fluctuations beyond the shot noise limit*, Ph.D. thesis, Gottfried Wilhelm Leibniz University (2024).
- [26] P. Kwee, C. Bogan, K. Danzmann, M. Frede, H. Kim, P. King, J. Pödl, O. Puncken, R. L. Savage, F. Seifert, et al., Stabilized high-power laser system for the gravitational wave detector advanced ligo, *Optics express* **20**, 10617 (2012).
- [27] H. Vahlbruch, D. Wilken, M. Mehmet, and B. Willke, Laser power stabilization beyond the shot noise limit using squeezed light, *Phys. Rev. Lett.* **121**, 173601 (2018).
- [28] M. G. A. PARIS, Quantum estimation for quantum technology, *Int. J. Quantum Inf.* **07**, 125 (2009).
- [29] T. Kessler, C. Hagemann, C. Grebing, T. Legero, U. Sterr, F. Riehle, M. Martin, L. Chen, and J. Ye, A sub-40-mhz-linewidth laser based on a silicon single-crystal optical cavity, *Nature Photonics* **6**, 687 (2012).
- [30] J. Dong, Y. Hu, J. Huang, M. Ye, Q. Qu, T. Li, and L. Liu, Subhertz linewidth laser by locking to a fiber delay line, *Applied optics* **54**, 1152 (2015).
- [31] S. Huang, T. Zhu, G. Yin, T. Lan, L. Huang, F. Li, Y. Bai, D. Qu, X. Huang, and F. Qiu, Tens of hertz narrow-linewidth laser based on stimulated brillouin and rayleigh scattering, *Optics Letters* **42**, 5286 (2017).
- [32] D. Matei, T. Legero, S. Häfner, C. Grebing, R. Weyrich, W. Zhang, L. Sonderhouse, J. Robinson, J. Ye, F. Riehle, et al., 1.5 μ m lasers with sub-10 mhz linewidth, *Physical review letters* **118**, 263202 (2017).
- [33] R. Finkelstein, S. Bali, O. Firstenberg, and I. Novikova, A practical guide to electromagnetically induced transparency in atomic vapor, *New Journal of Physics* **25**, 035001 (2023).
- [34] D. T. Weller, *Thermal Rydberg Spectroscopy and Plasma*, Ph.D. thesis, Universität Stuttgart (2019).

- [35] P. Williams, J. Hadler, F. Maring, *et al.*, Portable, high-accuracy, non-absorbing laser power measurement at kilowatt levels by means of radiation pressure, *Optics Express* **25**, 4382 (2017).
- [36] P. Pinot and Z. Silvestri, Optical power meter using radiation pressure measurement, *Measurement* **131**, 109 (2019).
- [37] A. M. Fox, *Quantum optics: an introduction*, Vol. 15 (Oxford university press, 2006).
- [38] P. Vaidyanathan, Generalizations of the sampling theorem: Seven decades after nyquist, *IEEE Transactions on Circuits and Systems I: Fundamental Theory and Applications* **48**, 1094 (2001).
- [39] I. I. Sobelman, *Atomic spectra and radiative transitions*, Vol. 12 (Springer Science & Business Media, 2012).
- [40] C. J. Foot, *Atomic physics*, Vol. 7 (Oxford university press, 2005).
- [41] A. Omont, On the theory of collisions of atoms in rydberg states with neutral particles, *Journal de Physique* **38**, 1343 (1977), eq.(4.3, 4.4).
- [42] B. Arora, M. Safronova, and C. W. Clark, Determination of electric-dipole matrix elements in k and rb from stark shift measurements, *Physical Review A—Atomic, Molecular, and Optical Physics* **76**, 052516 (2007).
- [43] C. Bahrim, U. Thumm, and I. Fabrikant, 3se and 1se scattering lengths for e-+ rb, cs and fr collisions, *Journal of Physics B: Atomic, Molecular and Optical Physics* **34**, L195 (2001).
- [44] I. Fabrikant, Interaction of rydberg atoms and thermal electrons with k, rb and cs atoms, *Journal of Physics B: Atomic and Molecular Physics* **19**, 1527 (1986).
- [45] M. Tanasittikosol, J. D. Pritchard, D. Maxwell, A. Gauguet, K. J. Weatherill, R. M. Potvliege, and C. S. Adams, Microwave dressing of rydberg dark states, *Journal of Physics B: Atomic, Molecular and Optical Physics* **44**, 184020 (2011).